

COMPUTATIONAL AND EXPERIMENTAL INVESTIGATION OF FLOW PARAMETERS IN THE ROTOR JET AT FLIGHT CONDITIONS WITH HIGH RELATIVE SPEED

Nikolay N. Tarasov and Valentina M. Shcheglova

Central Aerohydrodynamic Institute (TsAGI)
Zhukovsky Str., Zhukovsky, Moscow reg., 140160, Russian Federation
e-mail: xxx@tsagi.ru

Key words: rotor, vortex wake, average induced velocity

Abstract: Complex experimental and computational investigation of flow parameters in the rotor model wake for horizontal flight conditions have been performed. The computation results of deformed vortex sheet geometry behind rotor model are presented. The obtained computational wake shape is compliant with visualization results in flight tests and water channel of TsAGI. Based on the obtained deformations three components W_{xc} , \bar{W}_{yc} , \bar{W}_{zc} of time-averaged induced velocity in rotor wake at the distances from the rotor axis equal from $0.7R$ to $1.4R$ for flight conditions of $\mu=0.31$ are determined. Computational averaged induced velocities are compared with the results of velocity field measurements in the rotor model wake in the wind tunnel.

INTRODUCTION

Despite the fact that aerodynamic rotor blade loads have long been under studies the improvement of computational methods is the topic problem up to the present. Investigation of flow about a rotor in horizontal flight is not an easy problem both for the experiment and for the analytical solution. It is caused by imperfection of measurement techniques and mathematical methods. The experimental and theoretical studied of rotor operation should be performed in parallel with each other that is why only together they will help understanding the problem in spite of computational and experimental errors which can be considerable.

The practical value of any vortex theory of helicopter rotor in many respects is determined by the fact as far as the simplified models forming the basis of the computation theory reflect the actual laws of rotor vortex sheet formation. It can be shown only by comparison of experimental and computational results. Analysis of the rotor operation by the offered technique may be performed completely and quickly enough using the computer of moderate power.

Integrated and disturbed aerodynamic forces of the rigid rotor model with oblique flow around are computed using the program [1]. The computation of instantaneous and time-averaged induced velocities determined simultaneously with aerodynamic loads is performed based on the hypothesis of plane sections and steadiness in view of real blade section polar. Mutual influence of sections is caused by angles of induced wash near them. All induced velocity components both instantaneous and averaged in the wake are determined by nonlinear vortex theory [1]. The method is based on the use of the linear vortex theory in a first approximation and on the subsequent iteration process in the computation of rotor deformed free vortex wake. In the creation of the mathematical model the following assumptions were made: the effect of hub on flow around the rotor was ignored in determination of aerodynamic characteristics. Owing to insufficient computer power only five

turns of the spiral were taken into account in computation, and far wake corrections were not made.

1. TEST AND COMPUTATION OBJECT

The five-blade rotor model was tested with following geometrical and weight parameters: rotor diameter was $D=2.55$ m; flapping governor coefficient was $K=0$; solidity ratio was $\sigma=kb/\pi R=0.088$ (k – the number of blades, blade chord is $b=0.0865$ m); blade mass coefficient $\gamma=3.3$. The blade (set № 206) has rectangular plan form and an airfoil over the whole span NACA23010. Swashplate was at zero angle of attack. The experimental investigation of insulated rotor model in horizontal flight with relative speed $\bar{V}=V/\omega R=0.31$ at $C_t=0.0173$ and constructive angle of attack $\alpha_k=-14^\circ$ were made. The following flow parameters were determined: $\bar{W}=W/\omega R$ – a relative velocity in free-stream flow, $\Delta\alpha$ and $\Delta\beta$ – angles of flow wash.

The measurements are performed in wind-body coordinate system at the points with relative coordinates $\bar{x}=x/R$, $\bar{y}=y/R$, $\bar{z}=z/R$: $\bar{y}=0, \pm 0.078, \pm 0.156, \pm 0.234$; $\bar{z}=0, \pm 0.078, \pm 0.156, \pm 0.234, \pm 0.312, \pm 0.39, \pm 0.468, \pm 0.54$; at $\bar{y} \geq 0$ $\bar{x}=-1.01, -1.09, -1.17, -1.25, -1.325, -1.4$; at $\bar{y} < 0$ $\bar{x}=-0.7, -0.778, -0.855, -0.94, -1.01, -1.09, -1.17, -1.25, -1.325, -1.4$. Selected measurement region corresponds to the empennage and tail rotor position in the rotor wake at helicopter slip angle equal to $\pm 25^\circ$. The chart of measurement points is given in Fig.1.

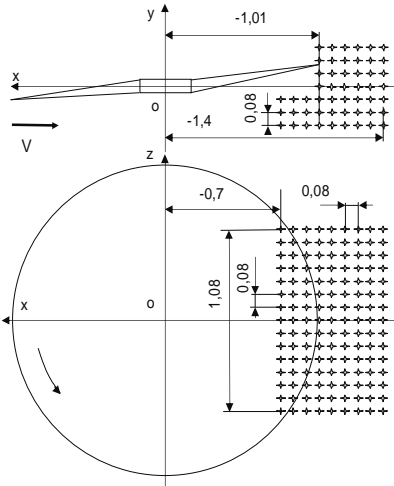


Figure 1: The chart of measurement and computation point location for $\mu=0.31$

The measurements were made using pitot-static tube by the technique described in [2]. Using the obtained in the experiment values of W , $\Delta\alpha$, $\Delta\beta$, the average induced velocities on the axes of wind-axes coordinate system \bar{W}_x , \bar{W}_y , \bar{W}_z were determined.

$$\begin{aligned}\bar{W}_x &= -\bar{V} + \bar{W}_{xy} \cdot \cos(-\Delta\alpha), \\ \bar{W}_y &= \bar{W}_{xy} \cdot \sin(-\Delta\alpha), \\ \bar{W}_z &= -\bar{W}_{xz} \cdot \sin(\Delta\beta),\end{aligned}\quad (1)$$

where: $\bar{W}_{xy} = \frac{\bar{W}}{\sqrt{1 + \operatorname{tg}^2 \Delta\beta \cdot \cos^2 \Delta\alpha}}$, $\bar{W}_{xz} = \frac{\bar{W}}{\sqrt{1 + \operatorname{tg}^2 \Delta\alpha \cdot \cos^2 \Delta\beta}}$, V is velocity in free-stream flow. The computed averaged induced velocities \bar{W}_{xc} , \bar{W}_{yc} , \bar{W}_{zc} are compared with experimental averaged induced velocities determined by the formulae (1).

To compute rotor effective angle of attack that influences the vortex sheet shape the blade flapping motion was determined. Blade flapping motion at each instant of the time ψ is described by equation:

$$\ddot{\beta} = \left[R^2 \int_{l_z}^1 \bar{T}(\bar{r} - \bar{l}_z) d\bar{r} - (\bar{I}_z \cos \beta - \bar{S}_z \bar{l}_z) \sin \beta - \frac{g}{\omega^2 R} \bar{S}_z \cos \beta \right] / \bar{I}_z \quad (2)$$

where: $\bar{T}=0.5 \cdot \rho \cdot \bar{W}^2 \cdot \bar{b} \cdot C_y$ – lift in blade section, \bar{W} – incoming flow velocity in blade section, \bar{b} – blade section chord, C_y – lift coefficient, $\bar{S}_z = R^2 \int_{l_z}^1 m(\bar{r} - \bar{l}_z) d\bar{r}$ – blade mass static

moment about flapping hinge, $\bar{I}_z = R^3 \int_{\bar{I}_z}^1 m(\bar{r} - \bar{I}_z)^2 d\bar{r}$ - blade mass moment of inertia about flapping hinge, I_z -flapping hinge stagger. The equation (2) is solved numerically to obtain $\beta(\psi)$ ranging from $\psi=0$ at the given initial conditions $\beta = \dot{\beta} = 0$ and integration step $\Delta\psi=5^\circ$. In computation of flapping motion at the given turn the information about blade motion and induced velocities at the previous turn is used. At the beginning of each turn the effective angle of attack is corrected. When swash plate is in the neutral position ($\theta_1=\theta_2=0$) and flapping governor is absent ($K=0$) the effective angle of attack is equal to $\alpha_e=\alpha_k+a_1$, where α_e - effective angle of attack, α_k -constructive angle of attack of the rotor, a_1 - turning angle of effective plane of rotation about constructive plane of rotation caused by flapping motion.

2. COMPUTATIONAL AND EXPERIMENTAL SHAPES OF VORTEX WAKE

A sufficiently great number of variants were calculated practically without complications associated with instability of the whole computational process and instability in determination of the induced velocities. Of some interest is a comparison of computational results by the method described in [1] with experimental data concerning both vortex sheet position in the space and averaged induced velocity values in the rotor vortex wake.

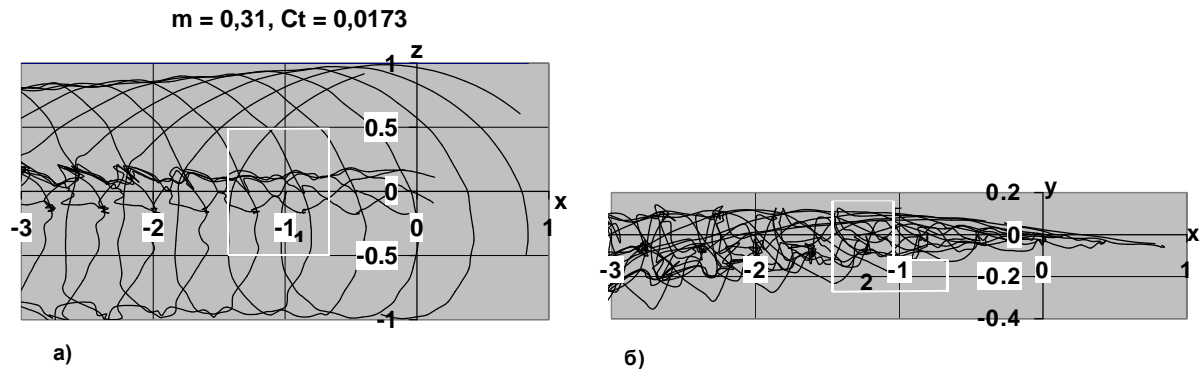


Figure 2: Locations of measurement and calculation regions in the vortex wake in the plane (a) and side (b) projections

The averaged induced velocities were calculated using computed deformed wake for $\mu=0.31$ the view of which is presented in Fig.2. For convenience of perception only tip and root vortices of each blade are shown. It should be noted that the positions of all free vortices shedding from the blade are determined in the computation. The root vortex wake (Fig. 2,a) lies between the sections $-0.176 < \bar{z} < 0.176$ and has a pronounced effect on induced velocities. It should be noted that all plots in Fig 2 defining the sheet shape are constructed for one of the variations by thickness parameter for blade vortices ε^2 where $\varepsilon=1/2\delta$, δ - vortex thickness. The main features of deformed wake shapes for all calculated variations by ε^2 are distinguished but little from those presented in Fig.2. Parameter ε^2 at the instant of sheet separation from blade surface under the assumption that the diffusion is absent was determined as:

$$\varepsilon^2 = 0.68^2 \cdot (0.15 \cdot C_{x_p}), \quad (3),$$

where: C_{x_p} - drag coefficient of the blade section equal to $C_{x_p} = 0.16 \cdot Re^{0.12}$.

The position of regions about the computed rotor vortex wake in which measurements and calculations were performed is also given in Fig 2.

The laws of rotor vortex wake formation illustrate the results of investigations on vortex sheet visualization [3, 4]. To compare qualitatively the computed results on determination the sheet shape by nonlinear model at $\mu=0.31$ the experimental data using smoke visualization of vortices shedding from blade tips at $\mu=0.306$ [3] are presented.

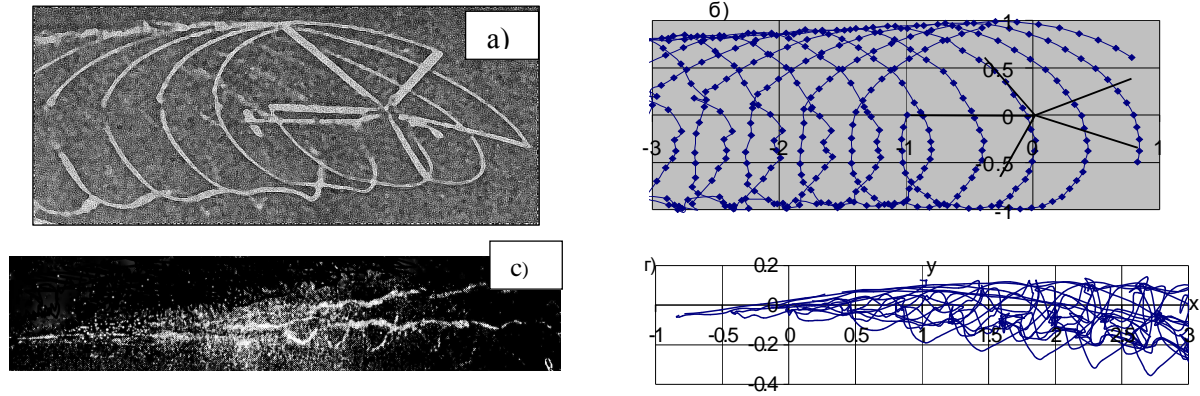


Figure 3: Experimental and computational shapes of vortex wakes for $\mu=0.31$: a) flight data, b) computation data, c) frames of rapid filming in water channel, d) computation.

The tip vortices take the form of cycloid which are deformed in time. However at high relative flight speeds due to slight secondary roll-up it is difficult to say definitely about the presence of longitudinal vortex cores in rotor wake though the accumulation of lateral deformed cycloids on the side of advancing blade resembles the longitudinal vortex in the plan view. The obtained computation geometry of the tip vortex agrees well with experimental form on all mentioned features (Fig.3,a, plan view).

Another example on visualization is presented in Fig. 3,c,d. Here the results on visualization of rotor vortex system using method of “cavitation” [4] are presented for five-bladed rotor in the horizontal flight at $\mu=0.3$. Cavitation bubbles in free vortices shedding from blade tips are conserved at a considerable distance from the rotor and well indicate the mechanism of vortex generation. The side projection of the wake obtained using the cavitation method and the side projection of calculated vortex wake are presented in Fig. 3,c and 3,d respectively. It is seen that qualitative agreement of computational and experimental results in Fig. 3 is satisfactory.

3. AVERAGED INDUCED VELOCITIES IN THE VORTEX WAKE

If the geometry of calculated deformed sheet and its spatial attitude behind the rotor are determined sufficiently accurate, then the potential of the computational method to predict the induced velocities nearby the rotor and in the wake more accurately increases. It is suggested that the computed loads and induced velocities should be near the real values on attainment of the given computation accuracy. This can be shown only by comparison of computational and experimental data. For this purpose the computation is carried out in the same points in which the measurements were made. To determine computed averaged velocities the vortex wake geometry was used (Fig. 2). To illustrate the obtained results as the example only the points in sites of great vortex accumulation at $\bar{y}=0$; -0.078 and -0.156 are considered. The time-averaged rotor induced velocity components W obtained in wind-tunnel test and in computation are compared here. These components are presented in Figs. 4, 5

($\bar{y}=0$), in Figs. 6, 7 ($\bar{y}=-0.078$) and in Figs. 8, 9 ($\bar{y}=-0.156$) as a function of \bar{z} coordinate in the range $\bar{z}=\pm 0.54$ for different distances from the rotor axis \bar{x} .

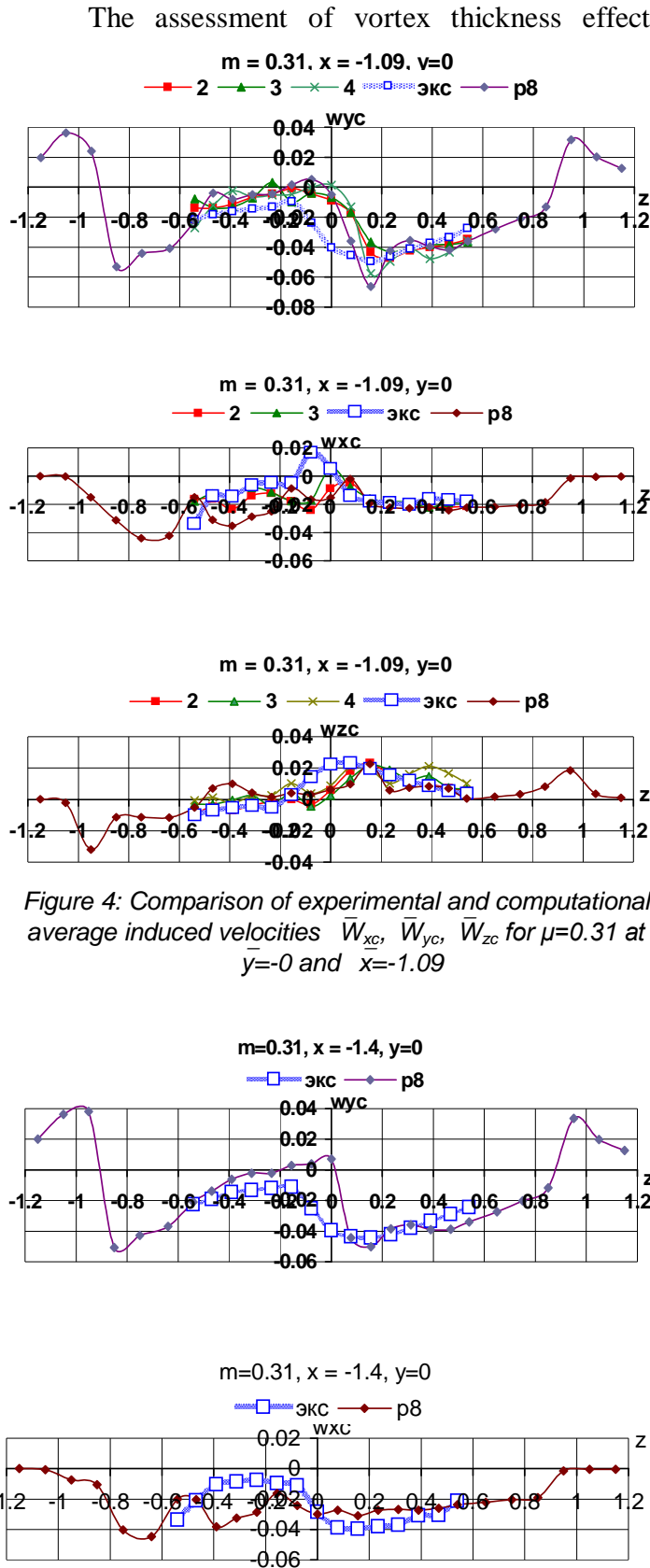


Figure 4: Comparison of experimental and computational average induced velocities W_{xc} , W_{yc} , W_{zc} for $\mu=0.31$ at $y=0$ and $x=-1.09$

The assessment of vortex thickness effect on computed induced velocities is performed. Four variants (2, 3, 4 and p8) differing from one another by vortex thickness parameter ε^2 (see Fig.4) were computed. For variants 2, 3 and 4 the parameter ε^2 was constant for all vortices except the tip vortex and was equal to 0.01 (variant 2), 0.001 (variant 3) and 0.0002 (variant 4). For the tip vortex ε^2 was equal to 0.0001 (variants 2 and 3) and 0.000085 (variant 4). For variant p8 parameter ε^2 is determined based on boundary layer thickness [1] in the instant of its shedding from blade trailing edge (3). This parameter depends on radius of calculated section that may be justified for high velocity regimes. The vortex thickness defined in such a manner for the variant p8 is lesser by an order of magnitude than for variants 4. As it is seen in Fig 4 the vortex thickness unquestionably affects the computation results, and the best agreement of computational and experimental induced velocities is obtained in computation of variant p8. In all other figures the computation results are presented only for the variant p8. The range of design points in variant p8 along axis z was expanded and varied from $\bar{z}=-1.15$ to $\bar{z}=1.15$.

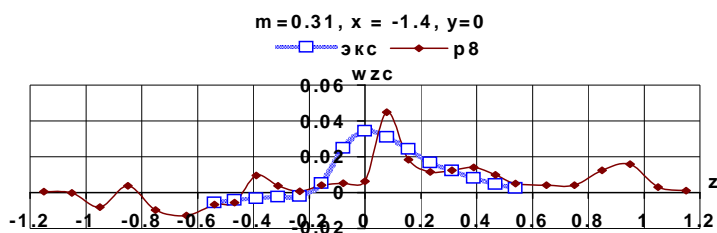


Figure 5: Comparison of experimental and computational average induced velocities \bar{W}_{xc} , \bar{W}_{yc} , \bar{W}_{zc} for $\mu=0.31$ at $\bar{y}=0$ and $\bar{x}=-1.4$

range from $\bar{z}=-0.2$ to $\bar{z}=0.2$. It may be explained by the following. Experimental measurements are made in disturbed and stagnant flow in the rotor model hub wake. In computation the presence of the hub is not simulated at all.

The stabilizer of some helicopters falls within the rotor wake area (Fig.4). Both

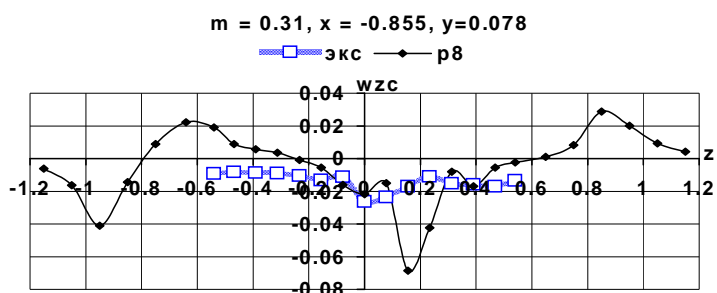
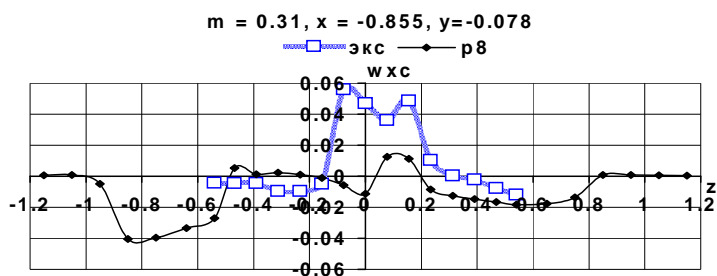
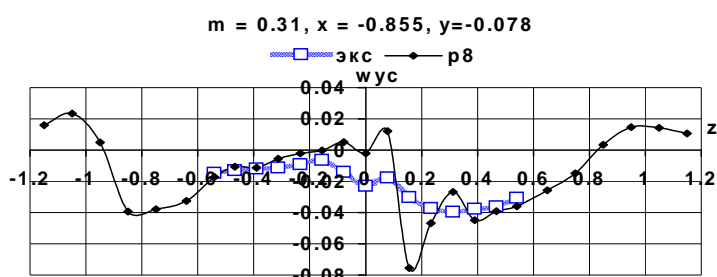


Figure 6: Comparison of experimental and computational average induced velocities \bar{W}_{xc} , \bar{W}_{yc} , \bar{W}_{zc} for $\mu=0.31$ at $\bar{y}=-0.078$ and $\bar{x}=-0.855$

$\bar{x}=-0.855$ are presented in Fig. 6. This area is located under rotor rotation plane. It is seen that the computational and experimental results are alike. The most significant differences are

In Fig 4 time-averaged relative induced velocity values of \bar{W}_{xc} , \bar{W}_{yc} , \bar{W}_{zc} at $\bar{y}=0$, $\bar{x}=-1.09$ are presented. It appeared that the computational and experimental results were found to be very like for all induced velocity components. It means that calculated induced velocity vectors correspond to experimental induced velocity vectors. The most perceptible differences are seen in the

experiment and computation show that at the studied regime when helicopter slip angle $\beta=0$ the stabilizer is flowed by very disturbed non-uniform flow. Induced velocities \bar{W}_{yc} are significantly different on the port and starboard stabilizer. In the case of helicopter slipping the whole stabilizer can be either in advancing blade wake ($\bar{z}>0$) when

$\bar{W}_{yc} \sim -0.04$ or in retreating blade wake ($\bar{z}<0$) when $\bar{W}_{yc} \sim -0.015$. Because of this, the longitudinal trim of the helicopter will be different.

The time-averaged relative induced velocity values of \bar{W}_{xc} , \bar{W}_{yc} , \bar{W}_{zc} at $\bar{y}=0$ and $\bar{x}=-1.4$ are presented in Fig. 5. The behavior of induced velocity distribution over the wake width at this distance from rotor rotation axis was much the same as in the case with $\bar{x}=-1.09$. The agreement of computational and experimental results is also satisfactory.

The time-averaged relative induced velocity values of \bar{W}_{xc} , \bar{W}_{yc} , \bar{W}_{zc} $\bar{y}=-0.078$ and

observed in the range from $\bar{z}=-0.2$ to $\bar{z}=0.2$. Essential flow deceleration in the wake behind rotor model hub and supporting devices is obtained experimentally in the studied area. In this case $\bar{W}_{xc}=0.06$ that runs about 20% of free-stream velocity. In computation the essential non-uniformity in the change of induced velocity components is obtained on the side of advancing blade ($\bar{z}>0$) in the range from $\bar{z}=0$ to $\bar{z}=0.3$. The plot in Fig. 2 can explain this result. It is seen that closeness of free root vortex cycloids is available on the side of advancing blade at $\bar{z} \sim 0.15 \dots 0.17$. By the location of these vortices it seen that they must have the most effect on induced velocity components \bar{W}_{yc} and \bar{W}_{zc} .

The time-averaged relative induced velocity values of \bar{W}_{xc} , \bar{W}_{yc} , \bar{W}_{zc} at $\bar{y}=-0.078$ and $\bar{x}=-1.4$ are presented in Fig 7.

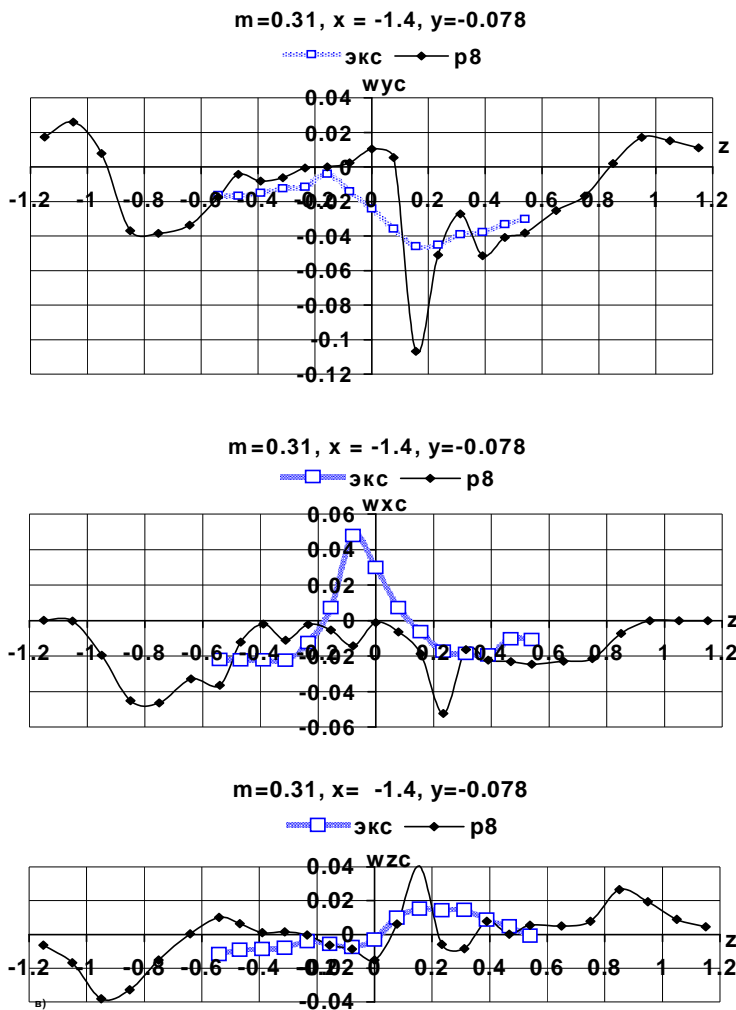
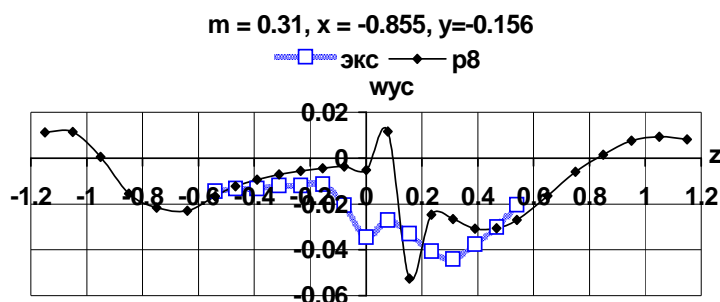


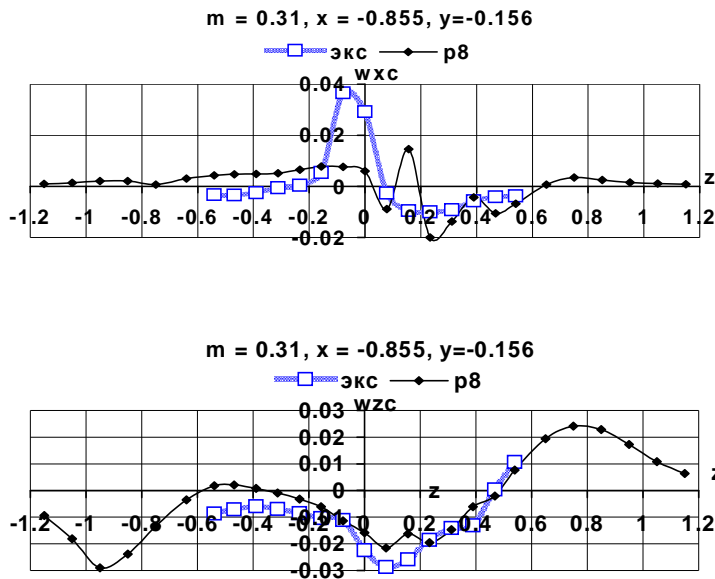
Figure 7: Comparison of experimental and computational average induced velocities \bar{W}_{xc} , \bar{W}_{yc} , \bar{W}_{zc} for $\mu=0.31$ at $\bar{y}=-0.078$ and $\bar{x}=-1.4$



The behavior of distribution of computational and experimental values of induced velocities \bar{W}_{xc} and \bar{W}_{yc} over the wake width at this distance from rotor rotation axis was much the same as in the case with $\bar{x}=-0.855$. Experimental values of \bar{W}_{zc} components on the side of advancing blade ($\bar{z}>0$) changed the sign and assume a character similar to the case with $\bar{y}=0$ (see Figs. 4 and 5). The obtained in computation essential effect on the induced velocities of free root vortices seems to be excessively significant and because of this the refinement of the computational model is required.

The time-averaged relative induced velocity values of \bar{W}_{xc} , \bar{W}_{yc} , \bar{W}_{zc} at $\bar{y}=-0.156$ and $\bar{x}=-0.855$ are presented in Fig. 8. This area is also located under rotor rotation plane. As distinct from the mentioned above

examples the computational and experimental results noticeably differ from one another in the range from $\bar{z}=-0.2$ to $\bar{z}=0.4$. Essential flow deceleration in the wake behind rotor model hub and supporting devices is obtained in the experiment in the range from $\bar{z}=-0.2$ to $\bar{z}=0.1$. In this case $\bar{W}_{xc}=0.04$ that runs about 13% of free-stream velocity. The



of \bar{W}_{xc} component prove it.

Figure 8: Comparison of experimental and computational average induced velocities \bar{W}_{xc} , \bar{W}_{yc} , \bar{W}_{zc} for $\mu=0.31$ at $y=-0.156$ and $x=-1.4$

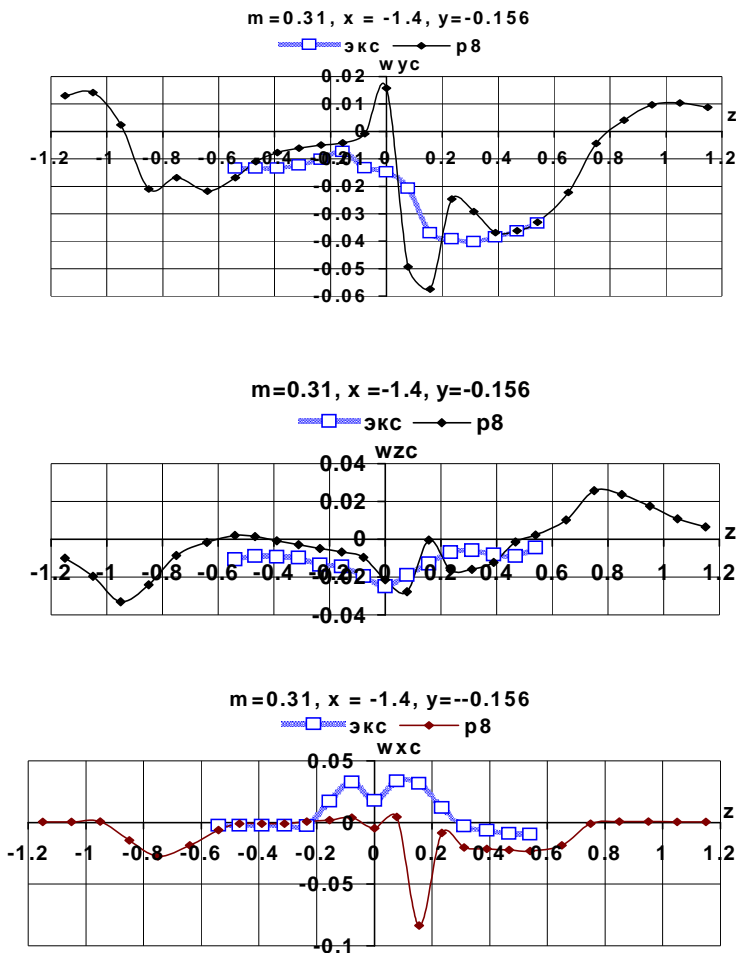


Figure 9: Comparison of experimental and computational average induced velocities \bar{W}_{xc} , \bar{W}_{yc} , \bar{W}_{zc} for $\mu=0.31$ at $y=-0.156$ and $x=-1.4$

essential non-uniformity in the change of induced velocity components \bar{W}_{xc} , \bar{W}_{yc} is obtained in computation on the side of advancing blade ($\bar{z}>0$) in the range from $\bar{z}=0$ to $\bar{z}=0.4$. It is seen (Fig. 2) that area of vortex sheet lower boundary with free vortices shedding from blade tips corresponds to the coordinates $\bar{y}=-0.156$ and $\bar{x}=-0.855$. It is possible that design points at $\bar{z}>0$ appeared inward the wake in the immediate vicinity to the wake boundary whereas on the side of retreating blade they appeared outward the wake. Positive values

The time-averaged relative induced velocity values of \bar{W}_{xc} , \bar{W}_{yc} , \bar{W}_{zc} at $\bar{y}=-0.156$ and $\bar{x}=-1.4$ are presented in Fig. 9. The behavior of distribution of computational and experimental induced velocities \bar{W}_{xc} and \bar{W}_{yc} over the jet width at this distance from rotor rotation axis was the same as in the case with $\bar{x}=-0.855$. Experimental values of \bar{W}_{zc} components on the side of advancing blade ($\bar{z}>0$) changed the sign and assumed a character similar to the case with $\bar{y}=0$ (see Figs. 4 and 5). The essential effect on computational induced velocities of free root vortices seems to be excessively significant and requires the refinement of the computational model.

Some general notes may be made for plots in Figs. 4-9. The comparison of computational and experimental results shows that the character of calculated curves well agreed with the character of experimental curves. Computation results satisfy experimental data on

the side of advancing blade in the

range from $\bar{z}=0.176$ to $\bar{z}=0.54$. The computed induced velocities at $|\bar{z}|>0.4$ practically coincide with experimental induced velocities both from the side of advancing blade and from the side of retreating blade. In pattern of observed differences between computational and experimental results it may be concluded that these differences appeared generally through the influence of disturbed and stagnant flow area with smeared boundaries in the hub and supporting devices wake downstream. For the given rotor this wake has the boundaries $\bar{z}\approx\pm 0.2$. As the rotor hub is not considered in the mathematical model the results of computation disagreed with experimental results in this area.

As a general conclusion it can be said that developed cod [1] makes it possible to determine vortex wake shape and average induced velocities caused by this wake with the use of the nonlinear model for the taken flight regime. Comparison of computational and experimental results illustrates the opportunity of this nonlinear model to predict average induced velocities in rotor vortex wake when the current wake geometry is defined exactly. The developed mathematical model gives satisfactory results in creating the practical nonlinear theory of helicopter rotor for high flight velocities and it can be used as the basis for further investigations in this area. The range of measurement points $-0.54\leq\bar{z}\leq 0.54$ presented in the experiment was inadequate and it is advisable to continue experimental investigations in wider range of flight regimes and coordinates.

CONCLUSIONS

1. The rotor model velocity fields are determined in the measurement points laying in the range $-0.54\leq\bar{z}\leq 0.54$ for the flight regime $\mu=0.31$.
2. Comparison of computational and experimental results was performed in investigations of rotor wake parameters. It is shown that the average induced velocities \bar{W}_{XC} , \bar{W}_{YC} , \bar{W}_{ZC} and the wake geometry determined for the nonlinear vortex model of rotor wake agree fairly well with experimental data at considered helicopter flight regime and primarily in the area of typical for single-rotor helicopter location of the tail rotor and empennage. Specifically, the computation results exactly reflect the presence of zones having higher velocities \bar{W}_{XC} than free-stream flow velocity \bar{V} ; the presence of stagnant flow zones as well as the appearance of the essential asymmetry of flow parameters and hence induced velocities about vertical longitudinal plane.
3. It is recommended: to use approved calculation method to account for the effect of the rotor on the aerodynamic characteristics of tail rotor and helicopter; to continue experimental investigations of rotor flow parameters in a wider space area and wider range of helicopter flight regimes; to improve the calculation method for the purpose of complete account of non-stationary and three-dimensional character of flow about rotor; to use the obtained results for rational choose of geometrical parameters and location of the empennage in developing aerodynamic configuration of single-rotor helicopter as well as in calculating trim, stability and control characteristics at the different flight conditions.

REFERENCES

- [1] Shcheglova, V.,M., "To Calculation of Rotor Induced Velocities on Nonlinear Model with Account to Vortex Diffusion" Uchenye Zapiski TsAGI, 2007, vol. XXXVIII, №3-4.
- [2] Antropov, V.,F., Burakov, G.,V., D'yachenko, A.,S. and Lipatov, V.,P. "Experimental Investigations on Helicopter Aerodynamics", M., Mashinostroenie , 1972.
- [3] Butov, V.,P. and Litvinov, B.,A., "Flight Tests of Rotor Vortex Wake for Coaxial and Single-Rotor Helicopter", Transactions of II Forum of Russian Helicopter Society

[4] Larin, A.,V. and Mavritsky, V.,I., “To Determination of Rotor Vortex System for Single-Rotor Helicopter at Horizontal Flight Regimes” Trudy TsAGI, issue 1226, M., 1970.

